Modeling of Turn-milling Process

Abstract

This paper presents an analytical approach for modeling of turn-milling which is a promising cutting process combining two conventional machining operations; turning and milling. This relatively new technology could be an alternative to turning for improved productivity in many applications but especially in cases involving hard-to-machine material or large work diameter. Intermittent nature of the process reduces forces on the workpiece, cutting temperatures and thus tool wear, and helps breaking of chips. The objective of this study is to develop a process model for turn-milling operations. In this article, for the first time, uncut chip geometry and tool-work engagement limits are defined for orthogonal, tangential and co-axial turn-milling operations. A novel analytical turn-milling force model is also developed and verified by experiments. Furthermore, matters related to machined part quality in turn-milling such as cusp height, circularity and circumferential surface roughness are defined and analytical expressions are derived.

Key Words: Turn-milling, Modeling, Cutting Force, Surface Quality

1. Introduction

Turning and milling operations are widely used conventional machining processes. Turn-milling is a relatively new process which combines turning and milling operations offering some clear advantages such as interrupted cuts and chip breaking [1]. Interrupted cutting decreases the contact time and allows the cutting tool to cool down which in turn reduces tool wear and increases tool life. Thus, turn-milling can offer increased productivity for difficult-to-machine materials such as high temperature alloys as well as parts with large diameters which cannot be rotated at high speeds.

Academic studies on turn-milling have started in 1990 by Schulz et al. who classified turn-milling operations in two categories: orthogonal and co-axial. This work dealt with eccentricity in orthogonal turn-milling, chip geometry and geometrical accuracy. Recent studies on turn-milling, on the other hand, have generally focused on surface quality of finished product. In their experimental study Choudhury and Mangrulkar [3] carried out a series of orthogonal turn-milling experiments on a vertical milling machine, obtained surface roughness data and compared it with those obtained by conventional turning. They found that the surface quality obtained by orthogonal turn-milling is 10 times better than those obtained by conventional turning. Choudhury et al. [4] studied again the surface roughness in orthogonal turn-milling but this time they compared the results with those obtained by conventional milling. In addition, they also predicted the surface roughness by means of experimental design. Another surface roughness study was done by Savas et al [5] who analyzed the surface roughness in tangential turn-milling achieving very good surface quality which is comparable to grinding. Kopac and Pogacnik [6] investigated the effect of eccentricity on surface quality in turn-milling concluding that surface roughness R_a in eccentric turn-milling is much better than that the one in centric turn-milling. Yuan and Zheng [7] tried to model the surface roughness and analyze the influencing factors emphasized the effect of eccentricity on surface roughness.

Besides surface roughness studies, Neagu et al. [8] analyzed the kinematics of orthogonal turn-milling from roundness, cutting speed and functional tool geometry point of views. As a conclusion they claimed that turn-milling can achieve up to 20 times higher productivity than conventional turning in roughing of straight shafts. In their study Kopac and Pogacnik [9] examined the effect of the entry and exit conditions, and found out that the tangential entrance was better for tool life.

Turn-milling has attracted more attention in recent years. In 2011 Filho [10] conducted orthogonal turn-milling experiments on a five axis machining center measuring cutting forces and comparing them with analytical model predictions for plunge turn-milling. Zhu [11] et al. developed two mathematical models that describe surface roughness and topography during orthogonal turn- milling and performed a series of experiments to verify the models, finally they proposed some parameter selection criteria based on theoretical and experimental result. Reduced tool wear is another advantage of turn-milling owing to intermittent cutting where cutting temperatures are expected to be low. Therefore, some researchers have investigated the effects of cutting parameters on tool wear in turn-milling [12, 13].

In this study, the major concern is to establish a comprehensive process model for orthogonal, tangential and co-axial turn-milling operations including chip thickness, kinematics, machined part quality and cutting forces. Therefore, for the first time in the literature uncut chip geometry and engagement limits are introduced at the outset for three types of turn-milling operation. Next, as an original contribution to the literature, cutting forces are evaluated by using uncut chip geometry and orthogonal cutting data. Moreover, the surface roughness is formulated for circumferential and axial directions. In addition, material removal rate (MRR) is specified and optimized by taking into account tool wear and machined part quality. The models and results presented in this work are believed to help understanding of turn-milling process geometry and mechanics as well as selection of process parameters better in order to increase productivity and part quality in these operations.

2. Uncut Chip Geometry

In order to understand the mechanics of turn-milling, firstly the chip formation is considered. Unlike conventional methods, in turn-milling chip removal is achieved by the combined rotations of both cutting tool and work piece. As a result, there are practically two feed rates; circumferential feed and axial feed. Circumferential feed is defined as the tool rotational motion around the work piece which is a result of the work piece rotation. Axial feed, on the other hand, is the translation motion of the cutting tool along the work piece. The combined motions of two feed rates result in a helical tool path as shown in Fig. 1.The parameters used to describe a turn-milling operation are summarized in Fig. 1 which illustrates depth of cut (a_p), feed per tooth (f_z), feed per workpiece revolution (a_e), eccentricity (e), number of tool revolutions (n_t), tool radius (R_t), workpiece radius (R_w) and number of workpiece revolution (n_w) and projected length of the tool onto workpiece (P_L). Fig. 1 also tells us that turn-milling can be defined by an analogy to conventional milling operation. If one assumes that the work piece is stationary and the tool moves around it, the circumferential feed (f_z) corresponds to the feed rate in conventional milling where axial feed (a_e) defines the radial depth of cut.
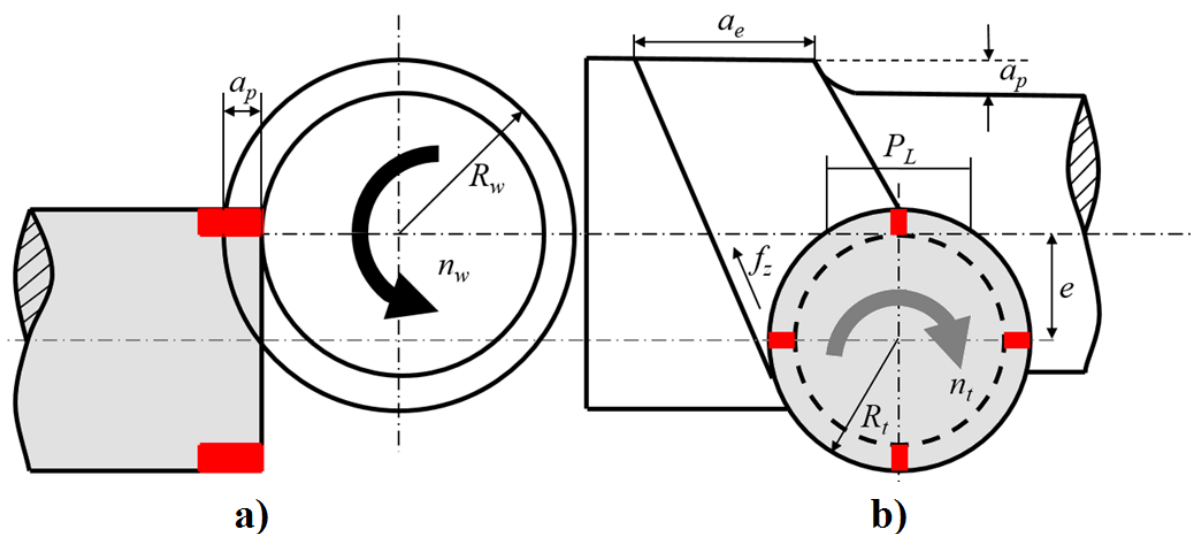
Fig. 1 Cutting geometry in turn-milling a) Side view of the process b) Top view of the process

2.1. Orthogonal Turn-Milling

In orthogonal turn-milling, the rotation axis of the cutting tool is perpendicular to the rotation axis of the work piece [4]. The chip is formed by both the bottom and the side of the tool in orthogonal turn-milling [10] as can be seen in Fig. 2a. The uncut chip geometry (Fig. 2b) is a fundamental need in process modeling, and can be obtained by considering the initial and the final positions of the tool within one tool revolution.
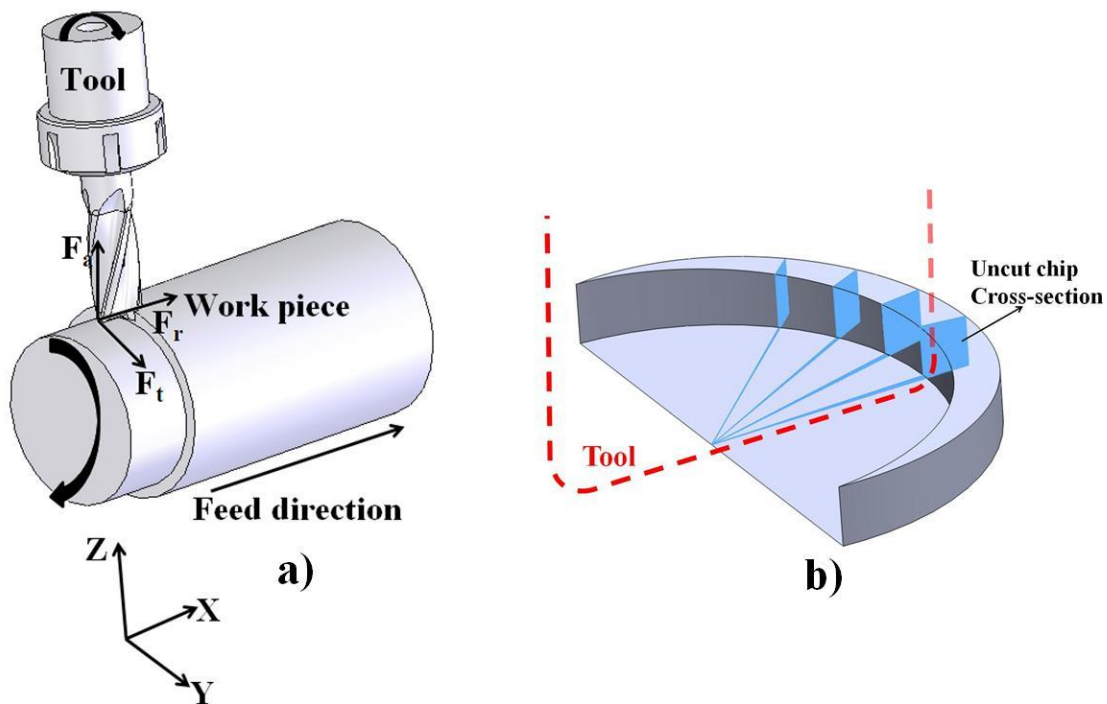
Fig. 2 a) Orthogonal turn-milling operation b) Uncut chip geometry in orthogonal turn-milling.

Fig. 3 shows the cross-section of the uncut chip. Points 1, 2 and 2' in Fig. 3 form envelop of the initial position of the cutting tool whereas points 1, 3 and 3' form the final position of the cutting tool in one revolution of the tool. The uncut chip cross-section area in Fig. 3 can be divided into two segments: the first segment is the lower section of the chip cut by the tool bottom face, and the second one is the higher section removed by tool side edge. Uncut chip geometry can be defined by geometrical relations of the lines 1-2, 1-3, 2-3 and θ which is the

angle between lines 1-2 and 1-3 representing the rotation of the tool around the work piece in one revolution of the cutting tool.
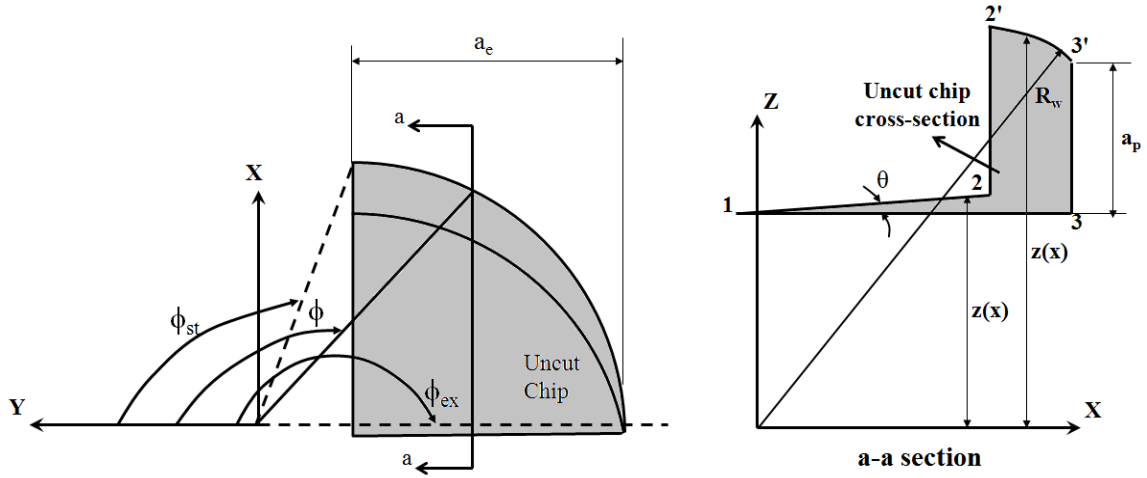
Fig. 3 The cross section of the uncut chip in orthogonal turn-milling.

Line 1-2 represents the bottom of the tool at the initial position and can be expressed by:

$$z(x) = \tan\theta.x + \frac{(R_w - a_p)}{\cos\theta} \tag{1}$$

where

$$\theta = \frac{2\pi}{m * r_n} \tag{2}$$

where x is the position along the X-direction, m is the number of cutting teeth and r_n is the ratio of n_t/n_w. The bottom of the tool at the final position in Fig. 3 corresponds to the line 1-3 and can be determined by:

$$z(x) = (R_w - a_p) \tag{3}$$

Arc 2'-3' is on the surface of the work piece:

$$z(x) = \sqrt{(R_w^2 - x^2)} \tag{4}$$

As mentioned before, there are two different regions on the uncut chip geometry; the limits of these two regions are determined by the points 1, 2 and 3:

$$x_1 = (R_w - a_p)\sin\frac{\theta}{2}$$
$$x_2 = (R_t - ((R_w - a_p) + \tan(\frac{\theta}{2})\tan\theta)\sin\theta)\cos\theta \tag{5}$$
$$x_3 = R_t$$

where R_t is the radius of the cutting tool. At this point one can compute the chip thickness at a desired location since each region has its own governing equation. In the first region which is bounded by lines 1-2 and 1-3, the chip thickness can be found as follows:

$$h(x) = \tan\theta.x + \frac{R_w - a_p}{\cos\theta} - (R_w - a_p) \tag{6}$$

The chip thickness in the second region which is formed by arc 2'-3' and line 1-3 can be formulated as:

$$h(x) = \sqrt{(R_w^2 - x^2)} - (R_w - a_p) \tag{7}$$

Another important parameter in determination of chip geometry is the feed per revolution which corresponds to the radial depth of cut in conventional milling. It directly determines the start and exit angles and can be seen in Fig. 3. The values of start and exit angles can then be found as:

$$\varphi_{st} = \frac{\pi}{2} + \arcsin\frac{R_t - a_e}{R_t} \tag{8}$$
$$\varphi_{ex} = \pi$$

2.2. Tangential Turn-Milling

Tangential turn-milling is another type of turn-milling operation in which cutting tool is tangent to the workpiece. As a result, unlike in the case of orthogonal turn-milling, in this case the chip is formed by only periphery of the cutting tool as shown in Fig. 4a. The procedure for determining the uncut chip geometry in Fig. 4b is similar to the case of orthogonal turn-milling.

a) **b)**
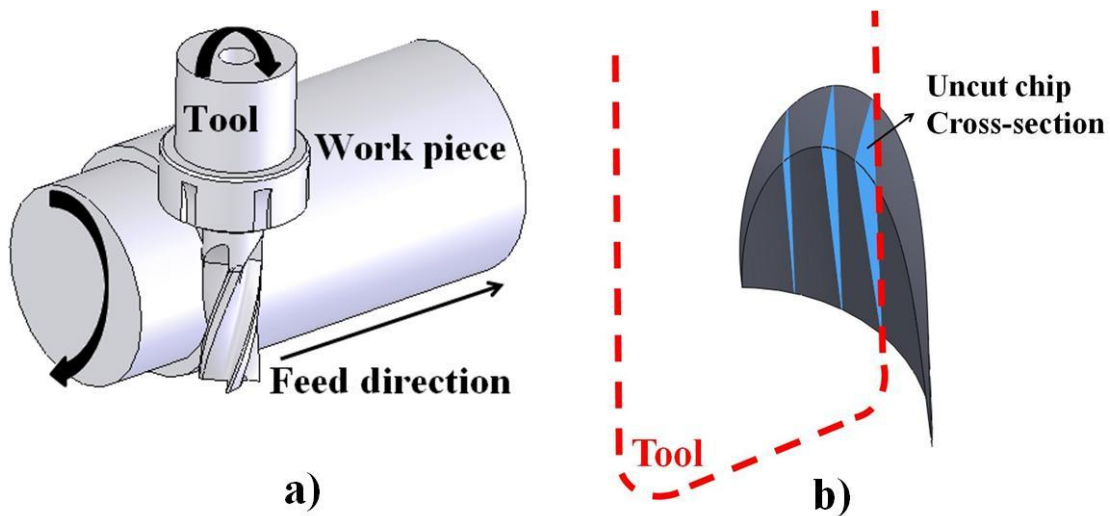
Fig. 4 a) Tangential turn-milling operation b) Uncut chip geometry in tangential turn-milling. Similar to orthogonal turn-milling the blue area in Fig. 4b indicates the chip cross-section. Lines 1-2, 1-3 and arc 2-3 in Fig. 5 are the boundaries of the uncut chip geometry. The angle θ is the same as in orthogonal turn-milling described by Eq. (2).
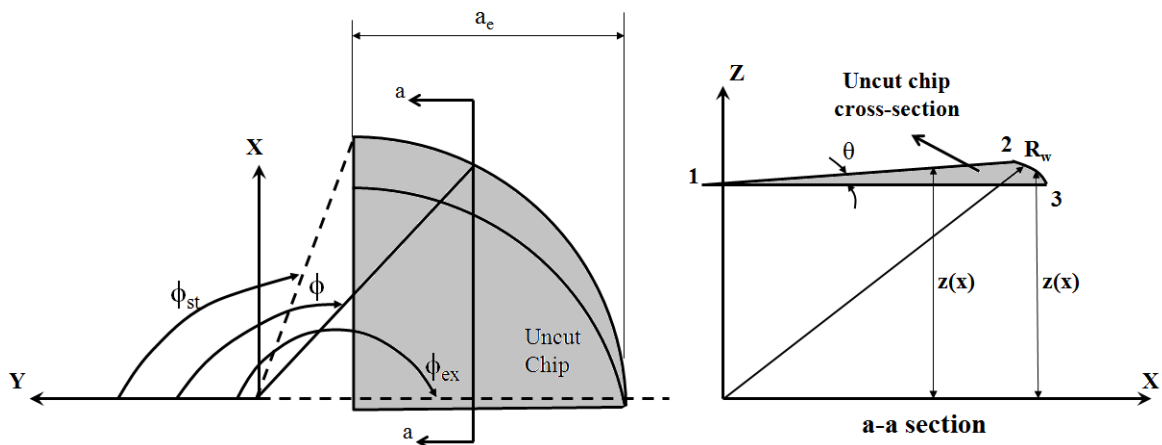
Fig. 5 Cross section of the uncut chip in tangential turn-milling.

Line 1-2 represents the initial position of the tool whereas line 1-3 represents its final position after a rotation of θ degree around the workpiece. Finally, arc 2-3 represents the portion of the workpiece.

The line 1-2 can be expressed as:

$$z(x) = \tan\theta . x + \frac{R_w - [\sqrt{R_t^2 - y^2} - (R_t - a_p)]}{\cos\theta} \tag{9}$$

Additionally, the equation for line 1-3 is:

$$z(x) = R_w - [\sqrt{R_t^2 - y^2} - (R_t - a_p)] \tag{10}$$

Finally, the arc 2-3 can be defined as:

$$z(x) = \sqrt{R_w^2 - x^2} \tag{11}$$

Similar to orthogonal turn-milling there are two different regions as shown in Fig. 5: the first one is up to point 2 and the second one is between points 2 and 3. Therefore, equations for the locations of these points should be derived:

$$\begin{aligned} x_1 &= -\left(\frac{\sin\theta(R_w - [\sqrt{R_t^2 - y^2} - (R_t - a_p)])}{\cos\theta + 1}\right) \\ x_2 &= \cos\theta\sqrt{R_w^2 - (R_w - [\sqrt{R_t^2 - y^2} - (R_t - a_p)])^2} \\ &\quad - (\sin\theta(R_w - [\sqrt{R_t^2 - y^2} - (R_t - a_p)])) \\ x_3 &= \sqrt{R_w^2 - (R_w - [\sqrt{R_t^2 - y^2} - (R_t - a_p)])^2} \end{aligned} \tag{12}$$

Finally, the start and exit angles can be defined as follows:

$$\varphi_{st} = \frac{\pi}{2} - \arcsin \frac{a_e / 2}{R_t}$$

$$\varphi_{ex} = \pi - \arcsin \frac{R_t - a_p}{R_t}$$

(13)

2.3. Co-axial Turn-Milling

In co-axial turn-milling tool and workpiece axes are parallel to each other. That's why only the periphery of the tool is in the cut. Fig. 6 describes the procedure for determining the uncut chip geometry for co-axial turn-milling. Unlikely the orthogonal and tangential turn-milling there is no linear boundary in co-axial turn-milling; the chip geometry in this case is formed by arcs.
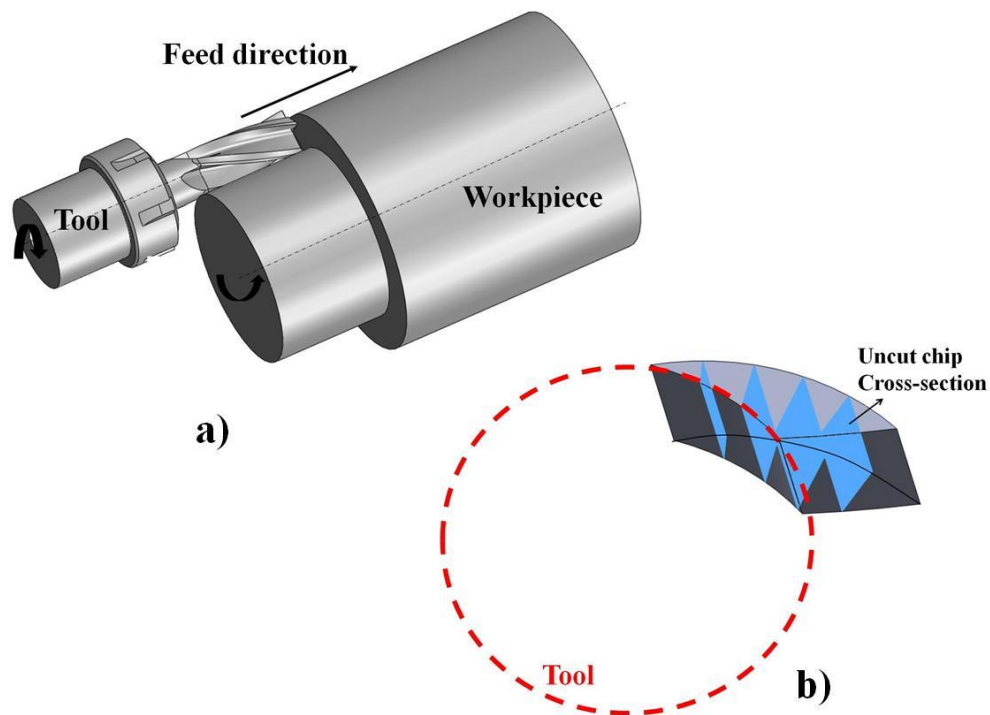
Fig. 6 a) Co-axial turn-milling operation b) Uncut chip geometry in co-axial turn-milling. Arcs represented by 1-2, 1-3 and 2-3 in Fig. 7 form the boundaries of the uncut chip. There are basically two different regions in co-axial turn-milling. The first one is limited by arcs 1-2 and 1-3 whereas the second region is limited by arc 1-3 and 2-3. In the first region chip thickness is represented by:

$$h = R_t - R_a \tag{14}$$

where

$$R_a = \frac{2(R_w + R_t - a_p)\sin(\theta/2)\cos((\pi - \theta) + \varphi)}{2} +$$

$$\frac{\sqrt{(2(R_w + R_t - a_p)\sin(\theta/2)\cos((\pi - \theta) + \varphi))^2 - 4((2(R_w + R_t - a_p)\sin(\theta/2))^2 - R_t^2}}{2} \tag{15}$$

Additionally in the second region

$$h = R_t - R_e \tag{16}$$

where

$$R_e = R_t - a_p + \frac{2\tan^2(\varphi)(R_t - a_p) - 2R_w}{2(1 + \tan^2(\varphi))\cos(\varphi)} -$$

$$\frac{\sqrt{(2\tan^2(\varphi)(R_t - a_p) - 2R_w)^2 - 4(1 + \tan^2(\varphi))\tan^2(\varphi)(R_t - a_p)^2}}{2(1 + \tan^2(\varphi))\cos(\varphi)} \tag{17}$$

Finally, the start and exit angles can be defined as follows

$$\varphi_{st} = \frac{\pi}{2}$$

$$\varphi_{ex} = a\tan\left(\frac{\sqrt{R_w^2 - \left[R_w - \left(\frac{R_t^2 - (R_t - a_p)^2}{2(R_t - R_w - a_p)}\right)\right]^2}}{R_t - a_p - \left(\frac{R_t^2 - (R_t - a_p)^2}{2(R_t - R_w - a_p)}\right)}\right) \tag{18}$$
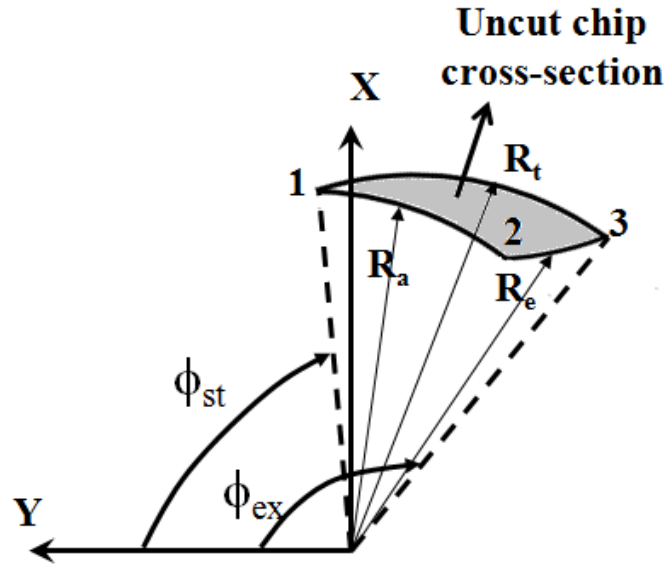
Fig. 7 The cross section of the uncut chip in co-axial turn-milling.

3. Turn-Milling Forces

Turn-milling is an intermittent cutting process which in turn causes periodic forces during cutting. Cutting forces in turn-milling are simulated using oblique transformation of orthogonal cutting data and the chip thickness expressions developed in Section 2 [14, 15]. For the orthogonal data used in the force coefficient calculations, true values of cutting conditions, such as local chip thickness and instantaneous cutting speed, are used in the calculations. Then, the turn-milling forces can be determined by dividing the uncut chip into elements within the cutting zone. The elemental cutting forces can be expressed as follows [15]:

$$dF_{t,j(\varphi,z)} = [K_{tc}h_j(\varphi_j(z)) + K_{te}]dz$$
$$dF_{r,j(\varphi,z)} = [K_{rc}h_j(\varphi_j(z)) + K_{re}]dz \qquad (19)$$
$$dF_{a,j(\varphi,z)} = [K_{ac}h_j(\varphi_j(z)) + K_{ae}]dz$$

K_t, K_r and K_a are the cutting coefficients and they are evaluated by oblique transformation to orthogonal cutting data. h is the chip thickness which is calculated by the procedure in Section 2. Finally, z is the axial depth of cut.
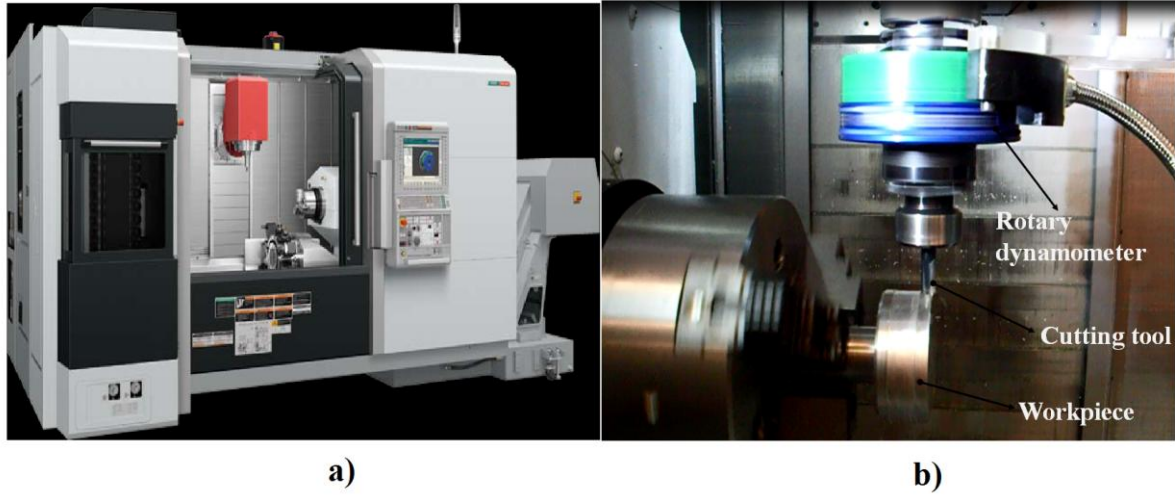
Fig. 8 a) Mori Seiki NTX 2000 machine tool and b) experimental setup for cutting forces.

The elemental forces are integrated within the engagement zone to obtain the total cutting forces as follows:

$$F_t(\phi_j(z)) = \int_{z_{j,1}}^{z_{j,2}} dF_t(\phi_j(z))dz$$

$$F_r(\phi_j(z)) = \int_{z_{j,1}}^{z_{j,2}} dF_r(\phi_j(z))dz \qquad (20)$$

$$F_a(\phi_j(z)) = \int_{z_{j,1}}^{z_{j,2}} dF_a(\phi_j(z))dz$$

where $z_{j,1}(\phi_j(z))$ and $z_{j,2}(\phi_j(z))$ are the engagement limits of the in-cut portion of flute j [15].

In order to verify the proposed model cutting experiments were performed on Mori Seiki NTX 2000 multi tasking machine tool which is seen in Fig. 8a. Measuring cutting forces during turn-milling operation is a challenge because both workpiece and tool rotate in case of cutting. Thus, a Kistler rotating dynamometer which is presented in Fig. 8b, was used in the experiments. Cutting tool was a 10 mm diameter solid carbide end mill with 4 teeth. Due to interrupted cutting, periodic forces occur in turn-milling. Fig. 9 shows experimental and

simulation results of orthogonal turn-milling of 1040 steel where cutting parameters were as follows; for Fig.4a n_t=2000 rpm, n_w=20 rpm, a_p=0.5 mm and a_e=0.3 mm/rev.
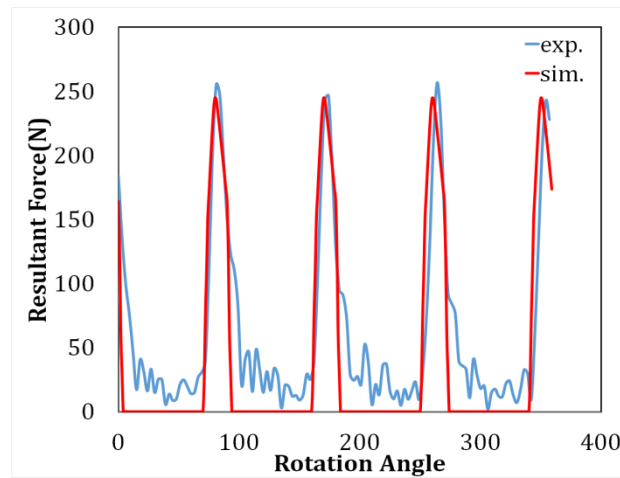
Fig. 9 Measured and simulated instantaneous cutting forces in turn-milling

In order to determine the effects of cutting parameters on turn-milling forces, cutting tests and simulations were performed using different values of r_n , a_p and a_e.

Table 1 Cutting conditions used in turn-milling tests.

Test No	R_w(mm)	R_t(mm)	n_t(rev/min)	n_w(rev/min)	r_n	a_p(mm)	a_e(mm)
1	45	5	3000	20	150	0.5	0.3
2	45	5	2000	20	100	0.5	0.3
3	45	5	2000	20	100	0.5	0.6
4	45	5	2000	20	100	1	0.6
5	45	5	4000	20	200	1	0.6
6	45	5	4000	20	200	1	0.3

Table 1 summarizes parameters used in the tests. The measured and simulated cutting forces for the conditions given in Table 1 are shown in Fig. 10. It can be observed that there is a good match between experimental and simulation results. Generally speaking cutting forces increase with the values of a_e and a_p, and decrease with r_n ratio.
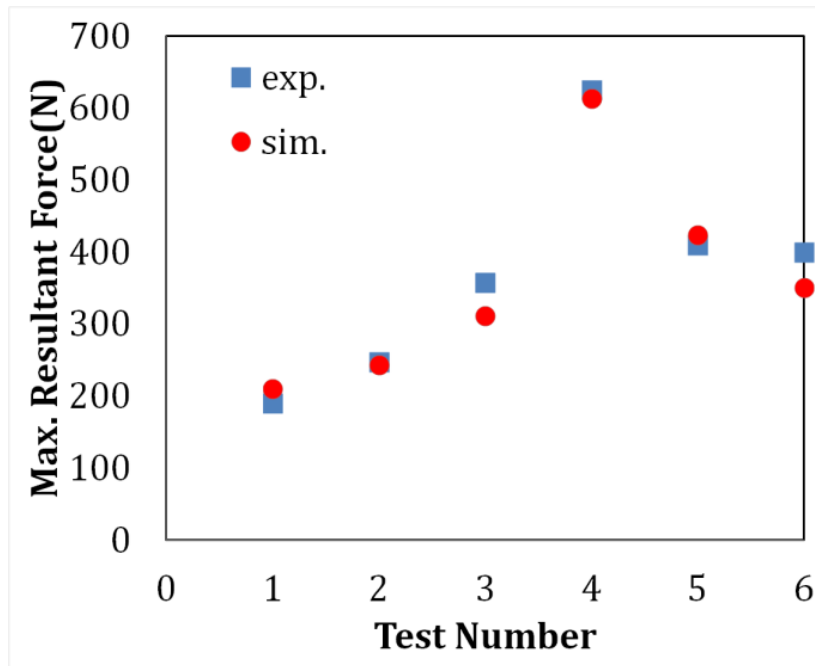
Fig. 10 Peak resultant forces for different cutting conditions.

4. Material Removal Rate in Turn-Milling

Manufacturing time, cost and quality of machined work pieces are affected by productivity and surface quality. Material removal rate (MRR) is an indicator of the productivity as it represents the removed material volume in unit time. Although turn-milling process potentially can generate high MRR, there are some drawbacks and limitations on it.
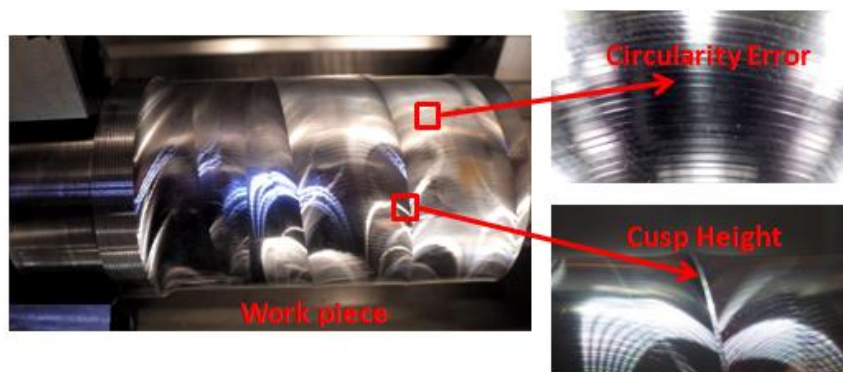
Fig. 11 Form errors in turn-milling

One of the main problems with increasing MRR in turn-milling is the form errors in circumferential direction as represented in Fig. 11. Due to the simultaneous rotations of both tool and work piece, the resulting machined cross section is a polygon as shown in Fig. 12a. In addition to the adverse effects of high MRR, cusp height may be observed on the machined

work piece especially for high a_e. The equation below represents the MRR for turn-milling process,

$$MRR = v_f * a_p * a_e$$
$$v_f = m * n_t * f_z$$

(21)

where a_e is the feed per work piece revolution, a_p is axial depth of cut and v_f is the feed speed and m represents the number of cutting edges.

5. Form Errors in Turn-Milling

5.1. Circularity

Turn-milling produces non–cylindrical surfaces due to the combined rotations of workpiece and tool. Fig. 12a shows obtained and desired forms in a turn-milling operation. As it can be seen from this figure the obtained form is a polygon. The difference between the desired circle and the scallop height denoted by *OB-OA* is the circularity error and can be formulated as follows:

$$OA = R_w - a_p$$
$$OB = \frac{R_w - a_p}{\cos \theta}$$
$$OB - OA = (R_w - a_p) * (\frac{1}{\cos \frac{\theta}{2}} - 1)$$

(22)
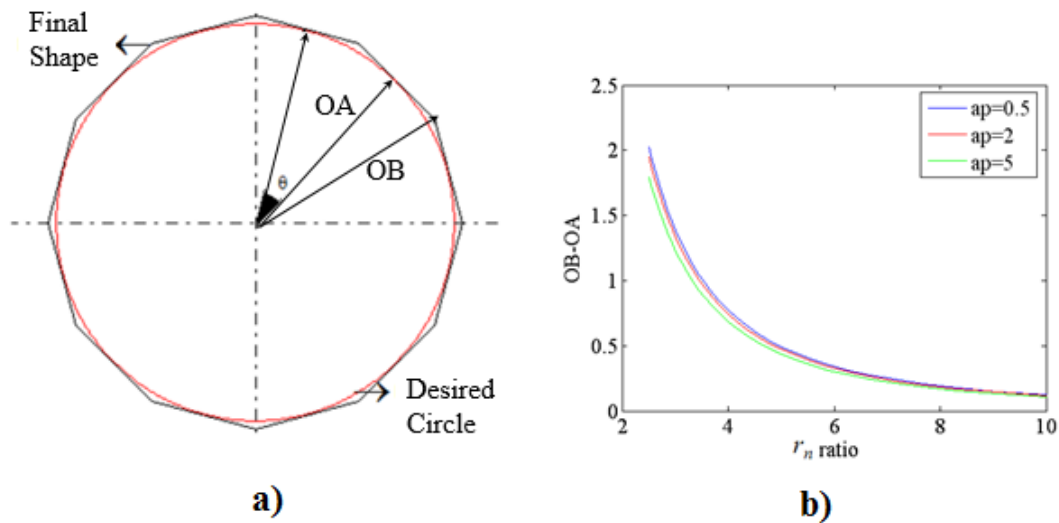
Fig. 12 a) Circularity error b) Circularity error with respect to a_p and r_n.

Eq. 22 indicates the relation between the cutting parameters and the circularity error. θ is the same angle in Eq. 2 and it includes r_n which is the rotational speed ratio of tool (n_t) and work piece (n_w), and number of teeth. Hence, one can optimize the circumferential surface roughness through selection of cutting parameters.

The effect of process parameters on circumferential surface roughness can be seen in Fig. 12b. It is obvious that r_n has a significant effect on circumferential surface roughness where the depth of cut has a slight effect. As a result, it can be suggested that the ratio of rotational speeds should be increased in order to improve circularity.

5.2. Cusp Height

Cusp which is another circumferential form error in turn-milling shown in Fig. 11, is the height of the remaining material on the surface due to the tool motion and directly associated with the tool and workpiece diameter as well as step over. Step over can be defined as the part of the cutter's diameter engaged in a cut. In conventional milling processes feed rate and cutting tool radius have direct effects on the cusp height. a_e in turn-milling process is equivalent to radial depth of cut in conventional milling process. Therefore, increasing a_e in order to achieve higher MRR, results in high cusp height.

Cusp height is derived as follows where the details are given in the Appendix.

$$ch = \sqrt{(R_w - a_p)^2 + \left(\left[e + \left[(R_w - a_p)*\tan\left(\frac{180°}{z*r_n}\right)\right]\right] - \left[\sqrt{(R_t)^2 - \left(\frac{a_e}{2}\right)^2}\right]\right)^2} - (R_w - a_p) \qquad (23)$$

where ch is cusp height, R_w radius of workpiece, e is eccentricity, m is number of cutting tool teeth and R_t is radius of cutting tool.

$$a_{ecrit} = 2*\sqrt{(R_t)^2 - \left(e + \left[(R_w - a_p)*\tan\left(\frac{180°}{z*r_n}\right)\right]\right)^2} \qquad (24)$$

a_e can be increased up to the critical value, which is represented by above equation, without producing any cusp. By this way, MRR can be increased without sacrificing surface quality. a_{ecrit} represents the projected length (P_L) of tool onto workpiece as shown in Fig. 1b. The derivation and details of Eq. 24 are given in the Appendix. If a_e is higher than this value, tool leaves uncut surface which is cusp height on the workpiece.
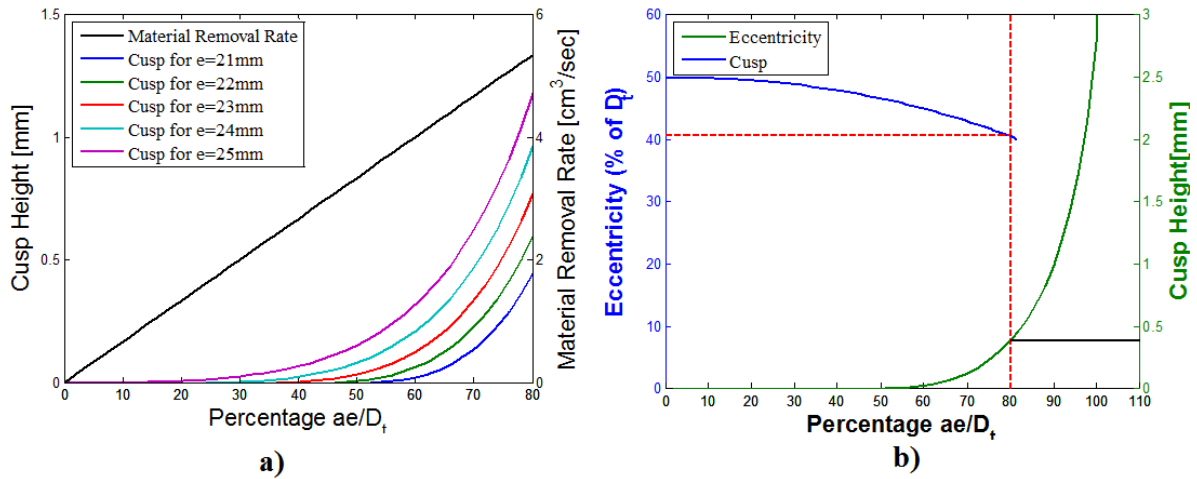
Fig. 13 Effects of turn-mill conditions on cusp height

Fig. 13a. illustrates eccentricity and feed per workpiece revolution effects on cusp height. The cutting parameters used in simulation are as follows; a_p=5 mm, R_w=50 mm, m=4, R_t=25 mm and r_n=200. According to the figure, the cusp height increases with eccentricity for the same a_e value. Since a_e affects both MRR and cusp height, it must be selected carefully. Fig. 13b illustrates variations of both a_e and cusp height for a selected eccentricity. When percentage a_e/D_t value is raised from 60% to 80%, both cusp and MRR are increased by 86% and 25% respectively.
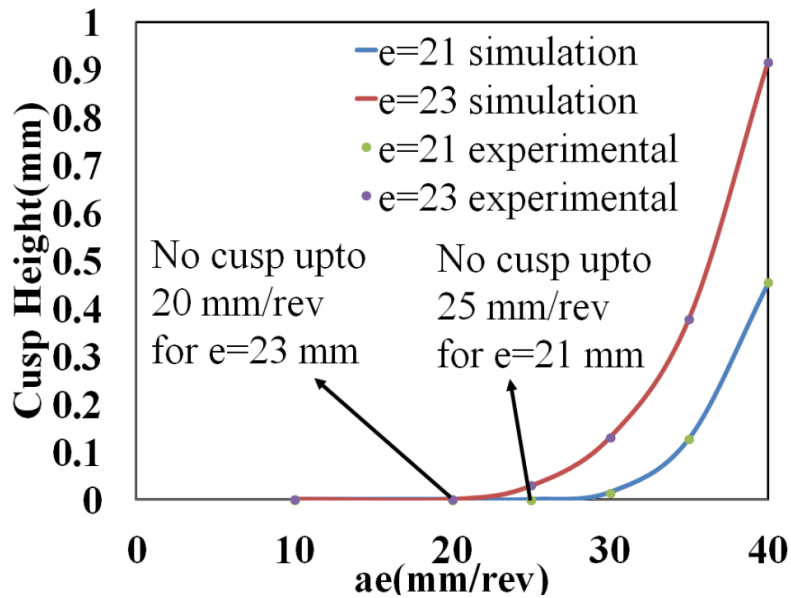
Fig. 14 Verification of the cusp height model with a_e and e effects.

Fig. 14 illustrates both analytical and experimental results for the cusp height. It can clearly be seen from the figure that up to a certain a_e there is no cusp regardless of the eccentricity. After that value, cusp increases dramatically.
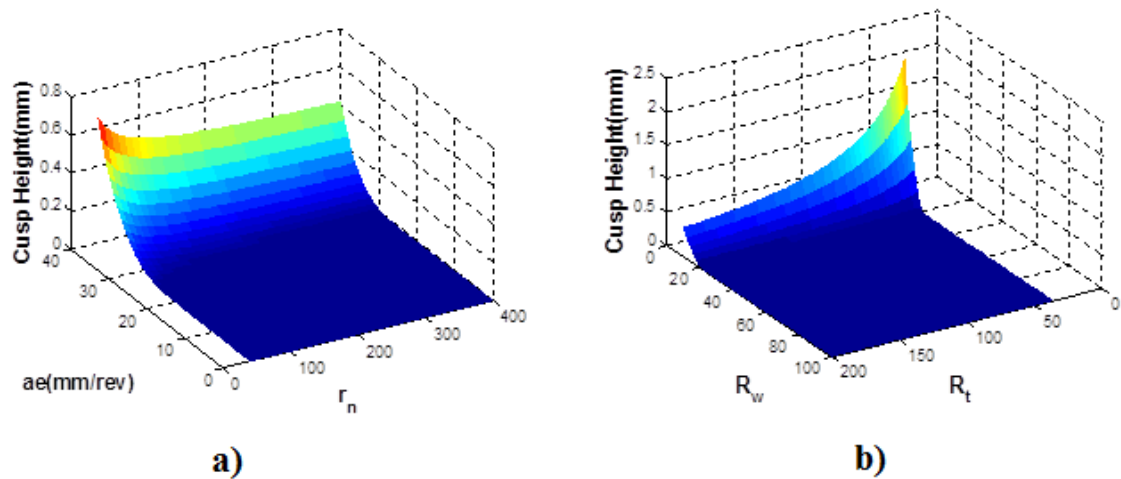
Fig. 15 Variations of cusp height.

Fig. 15 shows effects of a_e, r_n, R_w and R_t on cusp based on predictions by Eq. 23. Cutting parameters used in simulation are as follows; $a_p=5$ mm, $e=21$ mm, $m=4$, $n_t=2000$ rpm, $n_w=10$ rpm, $R_t=25$ mm and $R_w=50$ mm. It can clearly be observed from Fig. 15a. that increasing r_n results in decreasing cusp. In order to increase r_n, n_t can be raised which also increases MRR. According to Fig. 15b, tool radius has bigger effect than workpiece radius on cusp.

5.3. Circumferential Surface Roughness

Cutting tool follows a trochoidal path due to the simultaneous rotational movements of tool and work piece. The resulting feed marks on workpiece will be inclined through the machined length as illustrated in Fig. 16.
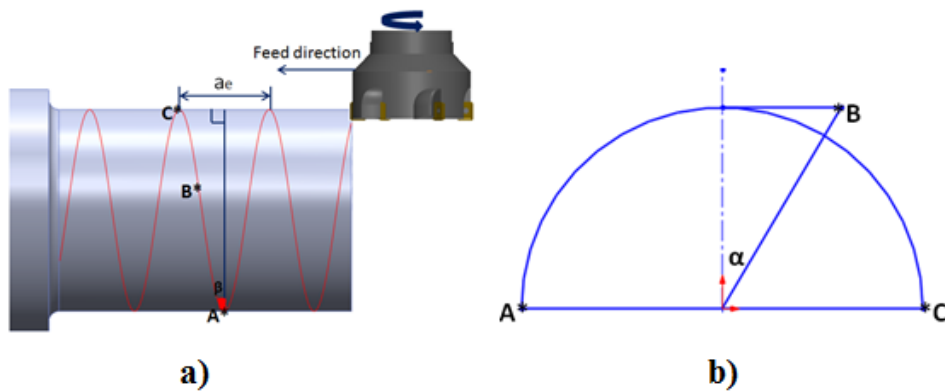
Fig. 16 Example tool path for turn-mill operation

The angle between this path and the normal line is indicated in Fig. 16a and can be derived as follows;

$$\beta = \arctan\left(\frac{a_e}{4*(R_w - a_p)}\right) \qquad (25)$$

Feed mark angle (β) effects the circumferential roughness dramatically. In circumferential surface roughness measurements, the probe or needle touches the workpiece at number of points which are at the same height from a base plane and equally located around the workpiece. As a result of this, the probe touches circular form errors and cusps because of the feed mark angle on the workpiece. The circumferential roughness is formulated as follows where the details are given in the Appendix.

$$circ_{rough} = \left(\frac{90° + \alpha}{180°}\right)*\left[\frac{(R_w - a_p)}{\cos(\theta/2)} - (R_w - a_p)\right] + \left(\frac{90° - \alpha}{180°}\right)*\frac{ch}{2} \qquad (26)$$

Circumferential surface roughness contains both cusp and circularity effects. The surface of the workpiece represented with three points named A, B and C as illustrated in Fig. 16b. Until point B, only circularity is observed on the workpiece. Between point B and C, cusp effect is involved in surface roughness calculations. Because of the workpiece is rotationally symmetrical, only half of the workpiece was taken into consideration. Point B represents the starting point of cusp height effect. From point B to C, cusp height increases linearly and at the end of the path it takes the maximum value. Moreover, from point A to B, only constant circularity can be observed on the machined workpiece surface. In other words, if the a_e is lower than a_{ecrit}, there will be only circularity form errors in the circumferential direction. The angle α which is represented in Fig. 16b, is calculated by the formula below;

$$\alpha = \arctan\left(\frac{\dfrac{\sqrt{(R_t)^2 - \left(e + \left[(R_w - a_p)*\tan\left(\dfrac{180°}{z*r_n}\right)\right]\right)^2}}{\tan\beta} - (R_w - a_p)}{(R_w - a_p)}\right) \qquad (27)$$

The derivation of angle α is given in the Appendix in detail.
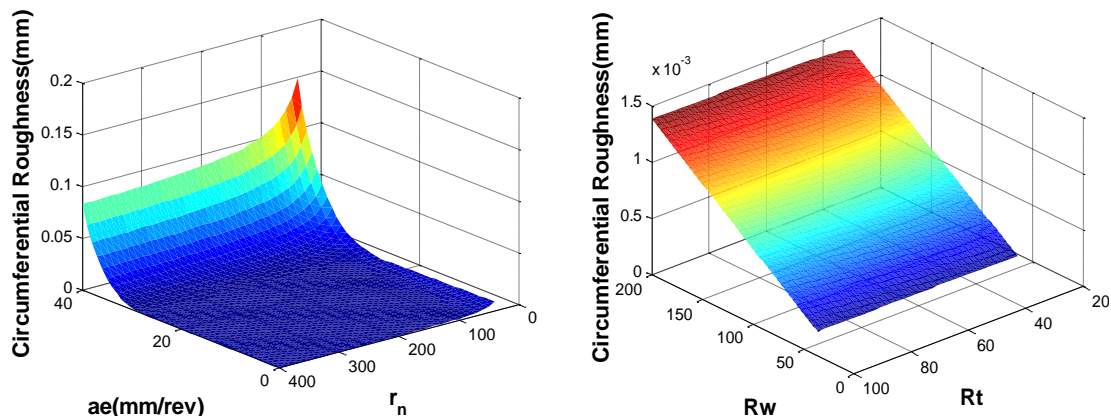
Fig. 17 Variations of circumferential surface roughness

Fig. 17 shows that increasing r_n and reducing a_e result in decreasing circumferential surface roughness. Moreover, workpiece radius has bigger influence on surface roughness than tool radius, as oppose to cusp height.

6. Conclusions

In this study, process models for turn-milling are introduced in order to achieve improved surface quality and material removal rate (MRR). Previous studies in the literature commonly include experimental investigations of surface roughness in turn-milling. In this paper, comprehensive formulations are introduced on geometry and mechanics of turn-milling for the first time. From theoretical and experimental studies performed in this research the following conclusions can be drawn:

1- Turn-milling is a relatively new machining process and the cutting parameters are different than those in conventional milling or turning. That is why a clear definition of the process geometry is necessary for better understanding of the process. For example, there are two feed rates in turn-milling. The circumferential feed (f_z) in turn-milling corresponds to the feed rate in conventional milling whereas axial feed (a_e) defines the radial depth of cut.

2- Uncut chip geometry and engagement limits are very important from cutting force, cutting temperature and stability points of view. Therefore, uncut chip geometry is introduced for orthogonal, tangential and co-axial turn-milling. The tool-workpiece contact area is defined and analytically calculated for instantaneous rotation angle of the cutting tool. The definitions developed for uncut chip geometry can be used for cutting force, temperature and stability analysis in turn-milling operations.

3- Based on chip geometry definitions, cutting force model is developed by using orthogonal cutting database and orthogonal to oblique transformation procedure. Cutting experiments were performed on a multi-tasking machine tool in order to verify the introduced model. Model and experiments results, which agree well with each other, show that cutting forces increase with a_p and a_e and decrease with r_n.

4-Turn-milling produces non cylindrical surfaces; in fact the resulting surface in turn-milling is a polygon. The degree of polygon strictly depends on the r_n ratio. If r_n ratio increases, the deviation from ideal circle decreases, which means that when tool rotates faster, the resulting surface approaches to an ideal circle and the circumferential surface roughness also decreases.

5-It is possible to achieve high MRR by turn-milling, however the part quality has to be taken into account as the parameters which affect the surface quality determine the MRR as well. Increase in a_e can improve MRR which comes at the cost of increased cusp height. On the other hand, it can be possible to turn-mill a part without cusp up to a certain value of a_e for a specific eccentricity value. As a result, MRR can be optimized according to the desired surface quality by using the analytical expressions derived in this paper.

6-As a result of simultaneous workpiece and cutting tool motions in turn-milling, the trajectory of the cutting tool on the workpiece is a helical path which causes variable circumferential surface roughness. The analytical expressions show that a_e and r_n have significant effect on the circumferential surface roughness. Up to a certain value of a_e the

circumferential roughness is equal to the circularity error and increases by decreasing r_n. However, beyond that value, the circumferential surface roughness increases dramatically by a_e.

7. References

[1] Turn-milling application overview, Sandvik Coromant. www.sandvik.coromant.com Accessed May 2014.

[2] H. Schulz, and G. Spur, High speed turn-milling—a new precision manufacturing technology for the machining of rotationally symmetrical workpieces, CIRP Annals-Manufacturing Technology. 39.1 (1990) 107-109.

[3] S. K. Choudhury, and K. S. Mangrulkar, Investigation of orthogonal turn-milling for the machining of rotationally symmetrical work pieces, Journal of Materials Processing Technology. 99.1 (2000) 120-128.

[4] S. K. Choudhury, and J. B. Bajpai, Investigation in orthogonal turn-milling towards better surface finish, Journal of Materials Processing Technology. 170.3 (2005) 487-493.

[5] S. Vedat, and C. Ozay, Analysis of the surface roughness of tangential turn-milling for machining with end milling cutter, Journal of Materials Processing Technology. 186.1 (2007) 279-283.

[6] J. Kopač, and M. Pogačnik, Theory and practice of achieving quality surface in turn milling, International Journal of Machine Tools and Manufacture. 37.5 (1997) 709-715.

[7] S. M. Yuan, and W. W. Zheng, The surface roughness modeling on turn-milling process and analysis of influencing factors, Applied Mechanics and Materials. 117 (2012) 1614-1620.

[8] C. Neagu, M. Gheorghe, A. Dumitrescu, Fundamentals on face milling processing of straight shafts, Journal of materials processing technology. 166.3 (2005) 337-344.

[9] M. Pogacnik, J. Kopac, Dynamic stabilization of the turn-milling process by parameter optimization, Proceedings of the Institution of Mechanical Engineers, Part B: Journal of Engineering Manufacture. 214.2 (2000) 127-135.

[10] C. Filho, J. Martins, Prediction of cutting forces in mill turning through process simulation using a five-axis machining center, The International Journal of Advanced Manufacturing Technology. 58.1-4 (2012) 71-80.

[11] L. Zhu, L. Haonan, W. Wansan, Research on rotary surface topography by orthogonal turn-milling, The International Journal of Advanced Manufacturing Technology. 69.9-12 (2013) 2279-2292.

[12] U. Karaguzel, U. Olgun, E. Uysal, E. Budak, M. Bakkal, High performance turning of high temperature alloys on multi-tasking machine tools, in New Production Technologies in Aerospace Industry, Springer International Publishing, 2014, pp. 1-9.

[13] C. Huang, Y. L. Cai, Turn-milling parameters optimization based on cutter wear, Advanced Materials Research. 602 (2013), 1998-2001.

[14] E. Budak, E. J. A. Armarego, Y. Altintas, Prediction of milling force coefficients from orthogonal cutting data, Journal of engineering for industry. 118.2 (1996) 216-224.

[15] Y. Altintas, Manufacturing automation: metal cutting mechanics, machine tool vibrations, and CNC design, second ed., Cambridge University Press, New York, 2012.

Appendix

Geometric Calculations for Turn-Milled Part Quality

1. **Cusp Height (ch) and Critical Feed per Workpiece Revolution (a_{ecrit}) Calculation (Equation 23 and 24 in the main text)**

Cusp is one of the important form error problems in turn-milling. The analytical formulation predicts that unlike the circularity form error, cusp height is an avoidable case. By using cusp height formulation, MRR and productivity can be increased without sacrificing any surface quality. Fig. A18a shows the cusp height formation on a turn-milled part in order to calculate the value of cusp height the illustrations in Fig. A18b and Fig. A18c can be used.
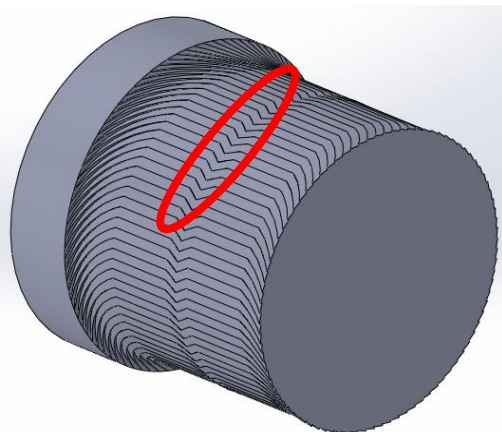
a) Isometric view of turn-milled part   **b)** Side view of turn-milled part
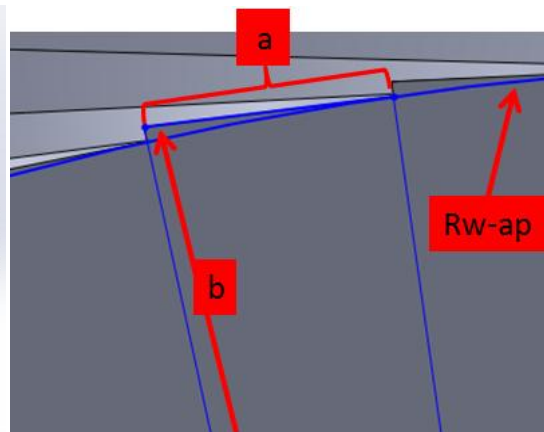
c) Top view of turn-milled part

Fig. A18 Cusp Height in Turn-milling

As shown in Fig. A18c;

$$a = \left(\left[e + \left[(R_w - a_p) * \tan\left(\frac{180°}{z * r_n} \right) \right] \right] - \left[\sqrt{(R_t)^2 - \left(\frac{a_e}{2} \right)^2} \right] \right) \tag{A.1}$$

From Fig. A18b;

$$b = \sqrt{(R_w - a_p)^2 + (a)^2} \tag{A.2}$$

Substituting Eq. A.1 into Eq. A.2;

$$ch = \sqrt{(R_w - a_p)^2 + \left(\left[e + \left[(R_w - a_p) * \tan\left(\frac{180°}{z * r_n} \right) \right] \right] - \left[\sqrt{(R_t)^2 - \left(\frac{a_e}{2} \right)^2} \right] \right)^2} - (R_w - a_p) \tag{A.3}$$

When a is equal to zero which means there is no cusp and given in Eq. A.1, critical feed per workpiece revolution value (a_{ecrit}) is obtained as;

$$a_{ecrit} = 2 * \sqrt{(R_t)^2 - \left(e + \left[(R_w - a_p) * \tan\left(\frac{180°}{z * r_n} \right) \right] \right)^2} \tag{A.4}$$

2. Circumferential Surface Roughness (*circ_rough*) & Angle "*α*" Calculation (Equation 26 and 27 in main text)

In order to calculate circumferential surface roughness in turn-milling, angle α must be determined because it indicates the location of point B on workpiece.
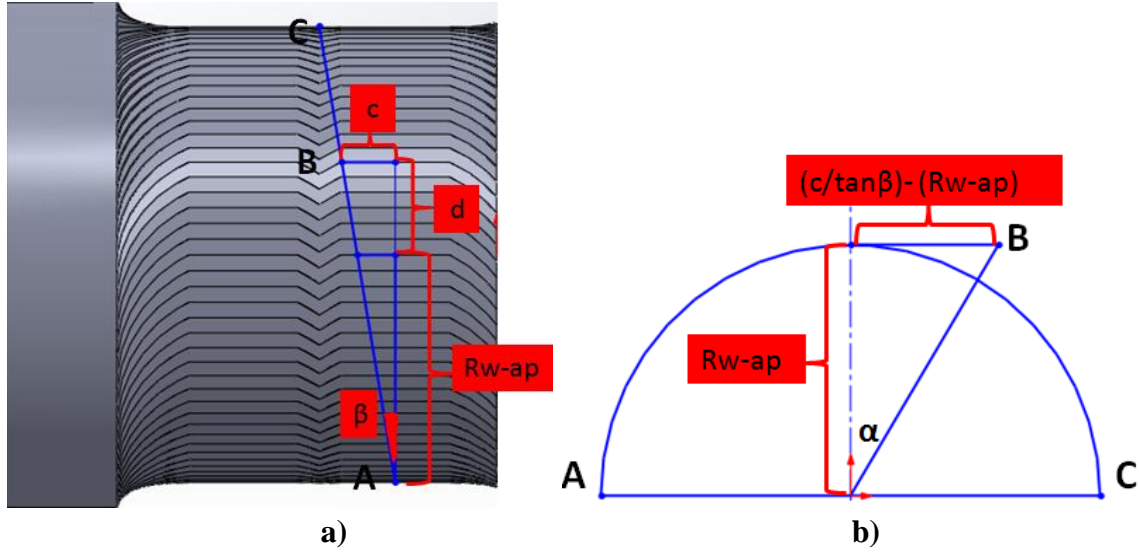
Fig. A19 Circumferential surface roughness in turn-milling

As illustrated in Fig. A19a, *c* represents half of the projected length ($P_L/2$);

$$c = \sqrt{(R_t)^2 - \left(e + \left[(R_w - a_p) * \tan\left(\frac{180^\circ}{z * r_n}\right)\right]\right)^2} \tag{A.5}$$

The vertical distance (*d*) between point B and workpiece center;

$$d = \frac{c}{\tan\beta} - (R_w - a_p) \tag{A.6}$$

And angle α is calculated as from the triangle represented in Fig. A19b;

$$\alpha = \arctan\left(\frac{\dfrac{\sqrt{(R_t)^2 - \left(e + \left[(R_w - a_p) * \tan\left(\frac{180^\circ}{z * r_n}\right)\right]\right)^2}}{\tan\beta} - (R_w - a_p)}{(R_w - a_p)}\right) \tag{A.7}$$

Surface roughness between points A and B;

$$circ_{rough} = \left(\frac{90^{\circ} + \alpha}{180^{\circ}}\right) * \left[\frac{(R_w - a_p)}{\cos(\theta/2)} - (R_w - a_p)\right] \tag{A.8}$$

From point B to C;

$$circ_{rough} = \left(\frac{90^{\circ} - \alpha}{180^{\circ}}\right) * \frac{ch}{2} \tag{A.9}$$

By using Eq. A.8 and Eq. A. 9, circumferential surface roughness;

$$circ_{rough} = \left(\frac{90^{\circ} + \alpha}{180^{\circ}}\right) * \left[\frac{(R_w - a_p)}{\cos(\theta/2)} - (R_w - a_p)\right] + \left(\frac{90^{\circ} - \alpha}{180^{\circ}}\right) * \frac{ch}{2} \tag{A.10}$$